# Reliability-based design for earth-fill dams against severe natural disaster events

Shin-ichi Nishimura, Toshifumi Shibata and Takayuki Shuku
*Graduate School of Environmental and Life Science, Okayama University, Japan*

ABSTRACT

The maintenance of geotechnical structures, such as earth-fill dams, is required as a countermeasure against severe natural disasters, namely, earthquakes, heavy rains. Since there is a recent demand for low-cost improvements, a reliability-based analysis is introduced here in response to this demand.

Firstly, a statistical model of *N* values is determined from Swedish weight sounding (SWS) tests to present the spatial variability of the soil strength. Secondly, a reliability-based analysis of embankments is conducted by considering the variability of the internal friction angle derived from *N* value, and the seismic hazard for the Nankai Trough. Thirdly, the probability of the overflow of earth-fills during heavy rains is evaluated. The rainfall intensity is dealt with as a probabilistic parameter, and the various rainfall patterns are tested by the proposed method. Finally, the total risk due to both earthquakes and heavy rains is evaluated for an earth-fill site. As a result, the possibility for the practical use of the proposed method in making plans for the maintenance of deteriorated earth-fill dams has been verified.

KEYWORDS: risk evaluation; earth-fill dam; damage probability; dam breaching; spatial variability; natural disaster; hazard curve; fragility curve; sounding test

## 1 INTRODUCTION

There are many earth-fill dams for farm ponds in Japan. Some of them are getting old and deteriorating, and therefore, have weakened. To mitigate disasters due to earthquakes and heavy rains, improvement works are being conducted on the most decrepit earth-fill dams. Since there is a recent demand for low-cost improvements, the final objective of this research is the development of a design method for optimum improvement works at a low cost. A reliability-based analysis is introduced here in response to this demand. The main purpose of this study is to present the reliability-based analysis considering both earthquakes and floods. The probabilistic modellings for the earthquakes and the rainfall are proposed simultaneously to evaluate the dam risks, and the approach is the novelty of this paper.

Many works related to the risk of dam breaching due to natural disasters have been published. Babu and Srivastava (2010) conducted a reliability analysis of earth dams, considering the soil's shear strength, horizontal seismic coefficient, and location of the full water level of the reservoir as the probabilistic parameters using response surface methodology. Xu and Zhang (2009) and Danka and Zhang (2015) dealt with dike breaching, and conducted a risk analysis for dams using the multiparameter nonlinear regression model of the main factors (dam height, reservoir shape coefficient, dam type, failure mode, and dam erodibility) to present dike breaching. Zhang *et al.*

(2009) also conducted a statistical analysis of a data base of dam failure cases. Foster *et al.* (2000) analyzed the statistics of the failure modes for dams, namely, the percentages of piping, slope failure, earthquakes, and overtopping. Rodriguez *et al.* (2017) evaluated the risk to dam systems brought about by the multiple-combination of the load system.

Recently, Bayesian statistics is often employed to assess the risk of dams. Wang and Zhang (2017) evaluated the probability of dam overtopping by using the Bayesian network model. Chen and Lin (2019) also made a risk assessment of a dam using the Bayesian network model. In particular, they evaluated the probability of overtopping due to multiple natural hazard sources. Many researchers, e.g., Sanmartin *et al.* (2019), Sharafati and Azamathulla (2018), Liu *et al.* (2018), and Zhong *et al.* (2018) have focused on the risk of dams by overtopping due to floods.

As the first task in this research, the damage probability due to severe earthquakes is evaluated. Firstly, statistical models for the $N$ values are determined from Swedish weight sounding (SWS) test results. In the present research, the spatial distribution of the strength parameters of decrepit earth-fill dams is discussed, and an identification method for the distribution is proposed. Although the strength of earth-fill dams is generally predicted from standard penetration test (SPT) $N$ values, SWS tests are employed in this research as a simpler method of obtaining the spatial distribution of the $N$ values. SWS tests are advantageous in that their simplicity makes short-interval exams possible. Secondly, the relationship between the SPT and the SWS $N$ values is modeled; it includes a transformation error term. The $N$ value distribution derived from the SWS tests is spatially simulated by the Monte Carlo Method (MCM).

To evaluate the probability of the failure of earth-fill dams, the circular slip surface (CSS) method is used along with the dynamic finite element method as the stability analysis method. The finite element method is used to estimate the normal and shear stress values on the slip surfaces during earthquakes. Then, the MCM is combined with the CSS method to obtain the probability of failure. The procedure for combining these two methods has also been conducted by, e.g., Shinoda, *et al.* (2006), Yoshida, *et al.* (2005), and Nishimura *et al.* (2016).

The strength parameter, namely, internal friction angle $\phi$, derived from the SWS tests, is considered to be the probabilistic variable. Additionally, two conversion error terms, namely, the error term from the SWS $N$ value to the SPT $N$ value and that from the $N$ value to $\phi$, are introduced to the MCM. Furthermore, the earthquake hazard of the Nankai Trough is considered in the reliability analysis. Then, the damage probability versus the earthquake acceleration level of an earth-fill dam is obtained.

As the second task in this research, the probability of overflow due to heavy rains is evaluated. Heavy rains comprise a very important factor in causing decrepit earth-fill dams to breach. Firstly, the quasi-rainfall intensities are generated from random numbers, based on the statistical rainfall model considering the sequence of the rainfalls. Secondly, the inflow and discharge are estimated considering the effect of the reservoir storage. When the peak overflow head on the spillway bed, $h_p$, becomes greater than the design overflow head, $h_d$, overflow occurs. Then, the probability of overflow $P_{fo}$ is calculated from the number of events, $h_p > h_d$, during the iterations of the MCM. Peak overflow head $h_p$ is determined within 72 hours of the rainfall, and the various rainfall patterns are tested by the MCM.

The generation methods of the rainfall are discussed in several works. Guzman and Oliver (1993) resented the generation method of the hourly precipitation with use of the first order Markov Chain model. Katz and Parlange (1995) applied the chain-dependent model based on the first order

Markov Chain to the hourly precipitations. Kottegoda *et al.* (2014) also simulated wet run (rainfall duration) and the dry runs base on the Markov Chain model with use of Monte Carlo simulation. Minagawa et al (2014) proposed the generator of the heavy rains purely based on the statistical distribution models.

In this work, a generator of the quasi- rainfall based on the Monte Carlo method is proposed with the similar concept of the referred works in the point that these approaches use the statistical models considering the correlation characteristics in the sequence of the rainfalls. While, the proposed approach is specified to assess the probability of overflow of the earth-fill dams by formulating the model from the 72 sequential hourly rainfall sensitive to the dam breaching.

As the third task in this research, the cost of damage to the downstream area due to the submergence brought about by the dam breaching, is estimated by a flood simulation based on the finite volume method. Finally, the total damage probability due to earthquakes and the overflow due to heavy rains through the lifetime period is obtained. The effect of improving an embankment is evaluated as the reduction in the risk of damage between the original and the restored states.

For engineering purposes, other factors should be addressed. Shear failure and piping failure should be considered in terms of heavy rains, and fault earthquakes, except for plate earthquakes, should be considered in terms of earthquakes. Only overflow failures and plate earthquakes, which can be supposed to be the dominant causes of dam breaches, are considered herein in order to present a simple approach to risk evaluation considering both heavy rain and earthquake events. To verify the effectiveness of the proposed scheme, Site H, located near Okayama City where a decrepit earth-fill dam exists, is analyzed here.

The flowchart to describe the overall procedure of the proposed approach is summarized in Figure 1. In the figure, the sections of this paper, in which each flowchart item is described, are indicated. Although the summarized concept of the approach was already presented by the authors (Nishimura *et al.* 2015), in this paper, more precise descriptions and the three flowcharts are included for the proposed approach to be applied easily for the future earth-fill dam design.

## 2 EARTHQUAKE HAZARD AND SAMPLE WAVE

The earthquake hazard curve is defined as the relationship between the maximum acceleration of an earthquake and the probability of exceedance during a specific period. In this study, the hazard data surrounding Site H, which is the object of the seismic analysis, have been obtained from the Japan Seismic Hazard Information Station (J-SHIS) (National Research Institute for Earth Science and Disaster Prevention). The hazard curve corresponding to maximum acceleration $a$, over the next 50 years, is depicted in Figure 2, which gives the probability distribution of the maximum acceleration. For the sequential value of the acceleration, hazard function $H(a)$ is determined. As an input seismic wave, a representative wave of the Nankai Trough Earthquake is used in this study (Cabinet office, Government of Japan); the wave is shown in Figure 3.

## 3 SEISMIC RELIABILITY ANALYSIS OF A FILL EMBANKMENT

### 3.1 Relationship between SWS $N$ and SPT $N$

Generally, the strength parameters are assumed based on standard penetration tests (SPTs) with

the use of empirical relationships. In this research, however, Swedish weight sounding (SWS) tests, which are simpler than SPTs, are employed instead of SPTs. Inada (1960) derived the relationship between the results of SPTs and SWS tests. Equation (1) shows the relationship for sandy grounds, while Figure 4 shows the relationship between the SWS results and the SPT $N$ values.

$$N_{SWS} = 0.002W_{SW} + 0.067N_{SW} \tag{1}$$

in which $N_{SWS}$ is the $N$ value derived from SWS, $N_{SW}$ is the number of half rations, and $W_{SW}$ is the total weight of the loads. Based on the data, the variability of the relationship is evaluated in this study, as the regression error, 0.354. The determined σ-limits are also shown in Figure 4 with broken lines. Considering the variability of the relationship, the SPT $N$ value, $N_{SPT}$, is modeled by

$$N_{SPT} = \left(1 + 0.354\varepsilon_r\right)N_{SWS} \tag{2}$$

in which $\varepsilon_r$ is an $N(0,1)$ random variable.

3.2 Analytical parameters in an earth-fill

A stability analysis is conducted and the risk is evaluated for an earth-fill dam at Site H. The soil profile for the embankment is categorized as intermediate soil. The mean function and the covariance function of the SWS $N$-values, $N_{SWS}$, are determined as follows. Details of the determination process are given in Nishimura *et al.* (2016). The mean function is determined as

$$m = 1.89 + 0.157z\,. \tag{3}$$

The covariance function is determined as

$$C_{ij} = 0.604\left(1.24\right)^2 \exp\left( -\frac{\left|y_i - y_j\right|}{6.14} - \frac{\left|h_i - h_j\right|}{0.63} \right) \quad \left(i \neq j\right)$$
$$C_{ij} = \left(1.24\right)^2 \quad \left(i = j\right) \tag{4}$$

where $y$ is the horizontal coordinate of the transversal direction of the embankment, $z$ is the depth from the ground surface, and $h$ is the elevation.

The analytical sections of the original embankment and the improved (restored) embankment at Site H, are presented in Figures 5 (a) and (b), respectively. The embankment has been improved by constructing an inclined core and by covering the original embankment with additional soil for reinforcement. The material properties are given in Table 1. The soil parameters are determined from the SPT $N$ values and laboratory soil tests. *Bs* means the embankment material; it is determined from the $N$ values based on the SWS test results instead of SPTs in order to consider the spatial distribution. The effective internal friction angle, $\phi' = \phi_d$, is obtained from the conversion, namely, Equations (5) and (6) (Hatanaka and Uchida 1996). In Equation (5), $3.0\varepsilon_f$ is the conversion error identified as the regression error of $\phi'$ and $\left(20N_1\right)^{0.5}$, in which $\varepsilon_f$ is an $N(0,1)$-type normal random variable and the ratio of 3.0 is the standard deviation.

$$\phi' = \left(20N_1\right)^{0.5} + 20 + 3.0\varepsilon_f \tag{5}$$

$$N_1 = N_{SPT} \Big/ \left(\sigma_v'/98\right)^{0.5} \tag{6}$$

in which $\sigma_v'$ is the effective vertical stress.

3.3 Reliability analysis

The circular slip surface (CSS) method is employed as the stability analysis in this study. Random numbers are assigned for uncertain factors, and the stability of the embankments is evaluated as the probability of failure with the use of the Monte Carlo method. For the reliability analysis, Equation (7) is defined as a performance function, in which the internal friction angle is a probabilistic parameter.

$$g = \sum_{i=1}^{n} \left( \tau_{fi} - \tau_{si} \right) l_i \tag{7}$$

where $\tau_f$ and $\tau_s$ are the shear strength and the shear stress, respectively, on the slip surface exhibited in Figure 6, which shows a slip surface across a finite element. In the figure, $l_i$ is the length of the slip surface of element $i$, and $n$ is the number of elements which a slip circle crosses. Strength $\tau_f$ is defined by Mohr-Coulomb's law given in Equation (8). Normal stress $\sigma_n$ and shear force $\tau_s$ are defined in Figure 6; they are calculated with the dynamic finite element method (LIQCA) (Uzuoka, *et al.* 2007) in this study. In the seismic response analysis, the linear-elastic model is employed for simplicity.

$$\tau_f = c' + \sigma_n' \tan\phi' \tag{8}$$

$$\sigma_n' = \frac{\left( \sigma_z' + \sigma_y' \right)}{2} + \frac{\left( \sigma_z' - \sigma_y' \right)}{2} \cos 2\theta - \tau_{yz} \sin 2\theta \tag{9}$$

$$\tau_s = \frac{\left( \sigma_z' - \sigma_y' \right)}{2} \sin 2\theta + \tau_{yz} \cos 2\theta \tag{10}$$

in which $c'$ is the effective cohesion, $\phi'$ is the effective internal friction angle, $\sigma_z'$ and $\sigma_y'$ are the vertical and horizontal stresses, respectively, $\tau_{yz}$ is the shear stress, and $\theta$ is the angle between the horizontal plane and the slip surface. In Figure 5, the highest potential slip surfaces are also presented. The stresses are dependent on earthquake acceleration $a$. The probability of failure is evaluated with Equation (11) through the use of the Monte Carlo method.

$$F_e(a) = \text{Probability}\left( g < 0 \right) \tag{11}$$

For the internal friction angle $\phi'$ of the embankment material, $Bs$ is dealt with as a random variable. Firstly, the random numbers considering the spatial distribution derived from Equations (1) and (2) are assigned to $N_{SWS}$. Secondly, random variable $N_{SPT}$ is evaluated by $N_{SPT} = N_{SWS}(1+0.354\varepsilon_r)$ by considering conversion error $\varepsilon_r$. Then, $\phi'$ is obtained with Equation (5), including the conversion error term, $3.0\varepsilon_f$. The Monte Carlo method is iterated 10,000 times.

In the calculation of the probability of failure $F_e(a)$, corresponding to maximum acceleration $a$, the level of the wave in Figure 3 is adjusted so that the maximum acceleration coincides with the target acceleration value. The fragility curves are obtained for the original and the restored embankments, respectively, as shown in Figure 7. For the original section, probability $F_e(a)$ reaches 100% at the acceleration of 1.5 (m/s$^2$), while, for the restored section, the probability

approaches 100% at around the acceleration of 3.0 (m/s$^2$). Considering hazard function $H(a)$, the damage probability due to earthquakes over the next 50 years, $P_{fe50}$, is defined as

$$P_{fe50} = -\int_0^\infty \frac{dH(a)}{da} F_e(a)\, da \tag{12}$$

The probability can be evaluated as 0.688 for the original state of the embankment and 0.429 for the restored state of the embankment.

In Figure 8, the flowchart of the seismic reliability analysis exhibited here to present overall procedure.

## 4. QUASI-RAINFALL MODEL

In this research, rainfall events continuing for 72 hours are simulated based on the annual maximum rainfall intensities obtained from the rainfall data records in Okayama City, Japan for a span of 45 years. A dam breach almost happens within 24 hours on an empirical basis. To cover all cases, the longer consecutive rainfalls of 72 hours are used. Examples of rainfall events are presented in Figures 9 (a) and (b). It can be understood from the figures that the heavy rains create various patterns on the hyetograph. The statistical modeling of the rainfall intensity is described in the following.

The cumulative distribution function $G_k(x)$ of rainfall intensity $x$ (mm/h), for $k$ (=1~72) hours after the rain starts, is determined with the mean rank method, given as

$$G_k(x) = m_k(x)/(N+1) \tag{13}$$

where $m_k(x)$ is the number of times the rainfall intensity after $k$ hours does not exceed $x$, and $N$ denotes the number of years. Figure 10 shows an example of the cumulative distribution of rainfall intensities.

Then, rainfall intensity $x$ (mm/h) is transformed into random variable $y$ following the standard normal distribution as

$$y = \Phi^{-1}(G_k(x)) \tag{14}$$

where $\Phi$ is the standard normal distribution function.

Then, correlation coefficients $\rho_{ij}$ ($i$,$j$ = 1, 2, …, 72), between probabilistic variable $y$ after $i$ hours and after $j$ hours, can be estimated by the following equation:

$$\rho_{ij} = \frac{\sum_{i=1}^{N} (y_i - \mu_i)(y_j - \mu_j)}{\sigma_i \sigma_j} \tag{15}$$

in which $\mu_i$ is the mean and $\sigma_i$ is the standard deviation, respectively, of component $i$.

Here, the set of correlation coefficients is viewed as a matrix, namely, $\mathbf{R} = [\rho_{ij}]$. The example for Okayama City is exhibited as follows:

$$\mathbf{R}=(\rho_{ij})=\begin{pmatrix} 1 & 0.66 & 0.50 & 0.15 & 0.11 & -0.06 & -0.05 & -0.17 & -0.12 & -0.13 \\ 0.66 & 1 & 0.55 & 0.34 & 0.35 & 0.06 & -0.10 & -0.17 & -0.04 & -0.05 \\ 0.50 & 0.55 & 1 & 0.66 & 0.46 & 0.14 & 0.02 & -0.09 & 0.07 & 0.07 \\ 0.15 & 0.34 & 0.66 & 1 & 0.69 & 0.46 & 0.28 & 0.24 & 0.31 & 0.13 \\ 0.11 & 0.35 & 0.46 & 0.69 & 1 & 0.58 & 0.34 & 0.27 & 0.33 & 0.22 \\ -0.06 & 0.06 & 0.14 & 0.46 & 0.58 & 1 & 0.78 & 0.51 & 0.49 & 0.40 \\ -0.05 & -0.10 & -0.02 & 0.28 & 0.34 & 0.78 & 1 & 0.74 & 0.62 & 0.50 \\ -0.17 & -0.17 & -0.09 & 0.24 & 0.27 & 0.51 & 0.74 & 1 & 0.66 & 0.48 \\ -0.12 & -0.04 & 0.07 & 0.31 & 0.33 & 0.49 & 0.62 & 0.66 & 1 & 0.79 \\ -0.13 & -0.05 & 0.07 & 0.13 & 0.22 & 0.40 & 0.50 & 0.48 & 0.79 & 1 \end{pmatrix} \tag{16}$$

*i, j* =1.2….10. The actual **R** has a size of 72×72 and Equation (16) presents the first 10×10 components.

Since **R** is positive definite, the lower triangular matrix **L,** satisfied with $\mathbf{LL}^{\mathrm{T}}=\mathbf{R}$, is obtained by the Choleky decomposition.

A normal random number, *Y*, can be produced as follows:

$$\mathbf{Y}=\mathbf{Lz} \tag{17}$$

where *z* is the standard normal random number generated by using the Box-Muller method (Rubinstein 1981). Then, using the following equation, normal random number *Y* is transformed into random number *X* which has the same distribution as the actual rainfall:

$$X_i = G_k^{-1}\left(\Phi\left(Y_i\right)\right) \tag{18}$$

If *X* is used directly as the quasi-rainfall, the pattern causing overflows may be fixed, because the cases of heavy rain events are very limited. To prevent the fixing of heavy rain patterns, a method is proposed whereby the rainfall intensity is decreased or increased, keeping the shape of the hyetograph.

The Gumbel distribution is assumed for the distribution of the total rainfall *T* (mm/72 hours) of the annual maximum 72 hours of rainfall, $f_G(T)$, determined as follows:

$$T=\sum_{i=1}^{72} x_i \tag{19}$$

$$f_G(T)=\exp(-e^{-w}) \qquad w=a(T-T_0) \tag{20}$$

where $x_i$ is the intensity of the annual maximum 72 hours of rainfall after *i* hours, and *a* and $T_0$ are the parameters employed to adjust the observed data to the theoretical distribution function (Iwai and Ishiguro 1970). Then, random variable $T'$ is generated as the total rainfall from Gumbel distribution $f_G(T)$ and is shown in Figure 11.

Lastly, the adjusted rainfall intensity, $X'$(mm/h), is determined for each hour with the following equation:

$$X'=(T'/\sum_{i=1}^{72} x_i)X \tag{21}$$

Two examples of generated rainfall series, generating 72 hours of rainfall, which are concentrating rainfall and long sequential rainfall patterns, are exhibited in Figure 12.

## 5. EVALUATION METHOD FOR THE PROBABILITY OF OVERFLOW

At first, the quantities of inflow, discharge, and storage are calculated. The inflow equation is defined as (JSIDRE 2015)

$$Q_{in} = f_p r A / 3.6 \tag{22}$$

where $Q_{in}$ is the inflow to the reservoir ($m^3/s$), $f_p$ is the peak runoff coefficient, $r$ is the quasi-rainfall intensity (mm/h) generated in Section 4, and $A$ is the area of the basin ($km^2$). Uniform random numbers are used for $f_p$ in the range of 0.7 to 0.8 (JSIDRE 2015). The discharge equation for a rectangular weir, as used in this study (Figure 13), is

$$Q_{out} = CB_S h^{2/3} \tag{23}$$

where $Q_{out}$ is the discharge ($m^3/s$), $C$ is the discharge coefficient, $B_s$ is the width of the spillway, and $h$ is the static or piezometric head on the weir referred to as the weir crest. The storage of water in the water reservoir, $V_r$, is estimated as follows:

$$V_r = A_w h \tag{24}$$

where $A_w$ is the area of the water reservoir ($km^2$) and $h$ is the overflow head (m). The decreasing rate of storage $V_r$ with the runoff is

$$dV_r / dt = Q_{in} - Q_{out} \tag{25}$$

Overflow head $h$ is determined from Equations (23) to (25), and the maximum $h$ within the 72 hours is defined as the peak overflow head on the spillway, $h_p$. When $h_p$ becomes greater than the design overflow head $h_d$, overflow occurs. Then, the probability of an overflow is defined by Equation (26) as the times of $h_p > h_d$ in the iterations of the Monte Carlo simulation (Rubinstein 1981). Rainfall intensity $r$, derived from $X'$, and peak runoff coefficient $f_p$ are random variables and considered as random numbers in the analysis.

$$P_{fo} = \mathrm{Prob}\left[ h_d < h_p \right] \tag{26}$$

The results for a dam at Site H are given in Table 2. In the table, the full water capacities, $V$, which flow out to the downward area are presented. The probability of overflow in a year, $P_{fo}$ is evaluated as 0.53% for the original state of the embankment and 0% for the restored state. The probability of overflow over the next 50 years can be estimated by Equation (27).

$$P_{fo50} = 1 - \left(1 - P_{fo}\right)^{50} \tag{27}$$

The value of $P_{fo50}$ at Site H is evaluated as 0.234 for the original embankment.

## 6. FLOOD SIMULATION

To determine the damage cost due to flood caused by the dam breach, the flood simulation is required. Based on the depth of submergence calculated by the flood simulation and the land use data, the damage cost can be estimated (Ministry of Agriculture, Forestry and Fisheries, Rural

Development Bureau 2015). The area, where the submerged depth is greater than 5 mm is assumed to be damaged in this study.

To conduct the flood simulation, the assumption of Rieman problem (Toro 1999), which can deal with the discontinuity of flow, is employed here. As basic governing equations, two-dimensional shallow water equations are employed, in which the flow velocity is assumed to be equally distributed along the vertical axis. Furthermore, the incompressibility of water and the inclined bottom are also assumed.

$$\frac{\partial \mathbf{U}}{\partial t}+\frac{\partial \mathbf{F}}{\partial x}+\frac{\partial \mathbf{G}}{\partial y}=\mathbf{S} \tag{28}$$

$$\mathbf{U}=\begin{pmatrix} h \\ uh \\ vh \end{pmatrix},\ \mathbf{F}=\begin{pmatrix} uh \\ u^2h+gh^2/2 \\ uvh \end{pmatrix},\ \mathbf{G}=\begin{pmatrix} uh \\ uvh \\ v^2h+gh^2/2 \end{pmatrix} \tag{29}$$

$$\mathbf{S}=\mathbf{S}_{\mathrm{o}}+\mathbf{S}_{\mathrm{f}}=\begin{pmatrix} 0 \\ ghS_{ox} \\ ghS_{oy} \end{pmatrix}+\begin{pmatrix} 0 \\ -ghS_{fx} \\ -ghS_{fy} \end{pmatrix} \tag{30}$$

in which $t$ is the time, $x$ and $y$ are the horizontal orthogonal axes, $h$ is the water depth, $u$ and $v$ are flow velocities for the $x$ and $y$ directions, respectively, $g$ is the acceleration of gravity, $S_{ox}$ and $S_{oy}$ are the inclinations along the $x$ and $y$ axes of the river bottom, respectively, and $S_{fx}$ and $S_{fy}$ are the inclinations of friction. Inclination $\mathbf{S_o}$ is obtained from the height of the bottom, $z_b$, and the positive direction of inclination is defined to be downstream, namely,

$$S_{ox}=-\frac{\partial z_b}{\partial x},\qquad S_{oy}=-\frac{\partial z_b}{\partial y} \tag{31}$$

The inclinations of the friction are defined from Manning's formula as

$$S_{fx}=\frac{n^2u\sqrt{u^2+v^2}}{h^{4/3}},\quad S_{fy}=\frac{n^2v\sqrt{u^2+v^2}}{h^{4/3}} \tag{32}$$

in which $n$ is Manning's roughness coefficient. The equations are solved by the finite volume method (FVM) (Yoon and Kang 2004), employing two-dimensional rectangular cells. The FVM is the numerical method based on the integral type equation, and the analytical area is divided into a finite number of cells. The group of cells that comprise the objective of the analysis is defined as the "control volume". An example of the control volume is exhibited in Figure 14. The cell arranged at the center of the control volume is defined as $L$, and the surrounding cells are defined as $R$ in the figure. Following this definition, the governing equation is derived as follows:

$$\frac{d\mathbf{U}_i}{dt}=-\frac{1}{\Omega_i}\sum_{j=1}^{4}\mathbf{E}\cdot\mathbf{n}_{ij}\Delta\Gamma_{ij}+\mathbf{S}_i \tag{33}$$

in which $\mathbf{E}=\mathbf{F}+\mathbf{G}$, $\mathbf{n}$ is unit normal outward vector, and $\Delta\Gamma$ is the length of the boundary. Numerical flux $\mathbf{E}\cdot\mathbf{n}$ is calculated by the HLL Rieman solver (Toro 1999) and expressed as follows:

$$\mathbf{E}\cdot\mathbf{n}=\begin{cases}(\mathbf{E_L})\cdot\mathbf{n} & (S_L\geq 0)\\ \dfrac{S_R(\mathbf{E_L})\cdot\mathbf{n}-S_L(\mathbf{E_R})\cdot\mathbf{n}+S_RS_L[(\mathbf{U_R})-(\mathbf{U_L})}{S_R-S_L} & (S_L<0<S_R)\\ (\mathbf{E_R})\cdot\mathbf{n} & (S_R\leq 0)\end{cases} \tag{34}$$

where $\mathbf{U}_L$ and $\mathbf{U}_R$ are the reconstructions of $\mathbf{U}$ on the left and right sides, respectively, and $S_L$ and $S_R$ are the wave speed estimates on the left and right sides, respectively.

$$S_L=\begin{cases}\min(\mathbf{q}_L\cdot\mathbf{n}-\sqrt{gh_L},u^*-\sqrt{gh^*}) & \text{if both sides are wet}\\ \mathbf{q}_L\cdot\mathbf{n}-\sqrt{gh_L} & \text{if the right side is dry}\\ \mathbf{q}_R\cdot\mathbf{n}-2\sqrt{gh_R} & \text{if the left side is dry}\end{cases} \tag{35}$$

$$S_R=\begin{cases}\max(\mathbf{q}_R\cdot\mathbf{n}-\sqrt{gh_R},u^*-\sqrt{gh^*}) & \text{if both sides are wet}\\ \mathbf{q}_L\cdot\mathbf{n}-\sqrt{gh_L} & \text{if the right side is dry}\\ \mathbf{q}_R\cdot\mathbf{n}-2\sqrt{gh_R} & \text{if the left side is dry}\end{cases} \tag{36}$$

$$u^*=\frac{1}{2}(\mathbf{q}_L+\mathbf{q}_R)\cdot\mathbf{n}+\sqrt{gh_L}-\sqrt{gh_R} \tag{37}$$

$$\sqrt{gh^*}=\frac{1}{2}(\sqrt{gh_L}+\sqrt{gh_R})+\frac{1}{4}(\mathbf{q}_L-\mathbf{q}_R)\cdot\mathbf{n} \tag{38}$$

in which $\mathbf{q}=[u\quad v]^T$.

In Figure 15, the overall flow chart of the flood simulation, is presented. Although the employed approach can be applied to evaluate the actual complicated shallow water flow to cause the floods, small time increment for the time steps is required to obtain the accurate solutions.

The Site H is modeled by the rectangular cells, of which size is 30m (lateral)×25m (vertical), numbers =11806, and the roughness coefficient is set to be 0.035. For simplicity, the whole bank of the dam is assumed to be breached instantly here.

In Figure 16, the results of the flood simulation for the downstream area of Site H are depicted; they present the maximum depth of submergence. The submerged area is limited to a narrow range, since the volume of the dam is not large.

## 7. RISK EVALUATION

### 7.1 Results of risk evaluation

The damage costs to the downstream area of Site H, according to the land use data, are presented in Table 3. The total damage cost for Site H is predicted to be 196 million JPY.

In Table 4, the damage costs due to earthquake and heavy rain events over the next 50 years are presented. Based on the probabilities, total damage probability $P_{all}$ is evaluated by Equation (39).

$$P_{all}=P_{fe50}+P_{fo50}-P_{fe50}\cdot P_{fo50} \tag{39}$$

The risk can be calculated by $P_{all}\times C_f$, in which $C_f$ (=196 million JPY) is the damage cost by submergence due to the dam breach. According to the table, the total risk is evaluated as 150 million JPY for the original embankment and 84 million JPY for the restored embankment. The

effect of the improvement work is reflected in the difference between the total costs of the original and the restored states, namely, 149,517-84,357=65,160 thousand JPY.

7.2 Effect of improvement works and future maintenance of earth-fill dams

The inclined core improvement work was selected in the analytical site. In the most major improvement works, the inclined core zone is installed, the spillway and the sluice pipe are newly constructed, and finally, the original embankment is reinforced by the cover soil as shown in Figure 5. Consequently, the probability of overflow is identified to be zero as presented in Table 2, since the increase of the ability for the spillway is very effective. In 2020 July Heavy Rain, no damage was observed for the improved earth-fill dams in Hiroshima and Okayama (Nishimura *et al.* 2020), and in result, the effectiveness of the improvement work currently employed was proved.

If the comparison of the improvement effects as such presented in Section 7.1 is conducted among many earth-fill dams, the earth-fill dams can be prioritized for the maintenance by the proposed approach, namely, the earth-fill dams which show the greater expected improvement effect can be given the higher priority.

## 8. CONCLUSION

(1) The SPT N values were derived from the SWS *N* values, and the internal friction angles were determined from the SPT N values, which can present the spatial distribution of the ground at Site H. Two conversion errors, from the SWS N value to the SPT *N* value and from the SPT *N* value to the internal friction angle, have been considered here.

(2) In terms of the seismic hazard for a Nankai Trough Earthquake, a reliability analysis has been conducted for an earth-fill embankment, and the damage probability over the next 50 years has been evaluated as 0.688 for the original state of the embankment and 0.429 for the restored state.

(3) A generation method for quasi-rainfall, using random numbers, has been proposed and applied for the rainfall records of Okayama City for the past 45 years. The generated precipitation events were applied to calculate the inflow from the surrounding basin into the reservoirs. The probability of overflow caused by heavy rains has been calculated for an earth-fill dam. It was assumed that overflows will occur when the maximum overflow head on the spillway bed becomes greater than the design overflow head. The probability of overflow over the next 50 years has been evaluated as 0.234 for the original state of the embankment and zero for the restored state.

(4) The damage costs of the downward area due to the case of submergence brought about by the breaching of the earth-fill dam by the flood simulation and the land use data have been evaluated.

(5) The total damage probability due to earthquake and heavy rain events over the next 50 years has been estimated as 0.76 for the original state of the embankment and 0.43 for the restored state. By comparing the risks between the original and the restored states, the effect of the improvement work has been clarified. The difference in the risks has been calculated as 65 million JPY.

(6) By the risk-based design, the earthquakes and the heavy rains can be considered simultaneously. Since the proposed procedure includes, the dynamic finite element analysis, the slip surface analysis, the flood simulation, and damage cost evaluation based on the land use data, great effort is required to complete the analysis for one site. To deal with the great number of earth-fill sites, more simplified approach is required. The proposed approach will be simplified by the

surrogate model (Nishimura *et al.* 2019).

ACKNOWLEDGEMENTS

This work has been supported by the Grant-in-Aid for Scientific Research (A), Grant Number 16H02577, of the Japanese Society for the Promotion of Science (JSPS). This support is gratefully acknowledged.

REFERENCES

Babu, G. L. S. and Srivastava, A.: Reliability Analysis of Earth Dams, Journal of Geotechnical and Geoenvironmental Engineering, 136(7), https://doi.org/10.1061/(ASCE)GT.1943-5606.0000313, 2010.

Cabinet office, Government of Japan, Information page for disaster prevention, http://www.bousai.go.jp/jishin/nankai/

Chen, Y and Lin, PZ ., Bayesian network of risk assessment for a super-large dam exposed to multiple natural risk sources, Stochastic Environmental Research and Risk Assessment, 33(2), 581-592, 2019.

Danka, J. and Zhang, L.M., Dike Failure Mechanisms and Breaching Parameters, Journal of Geotechnical and Geoenvironmental Engineering, 141(9), 1957-1970, 2015.

Foster, M., Robin Fell, R. and Spannagle, M., The statistics of embankment dam failures and accidents, Canadian Geotechnical Journal, 37(5), 1000-1024, 2000.

Guzman, A.C. and Oliver, E.A., A stochastic model of dimensionless hyetograph, WRR, 29(7), 2363-2370, 1993.

Hatanaka M. and Uchida A., Empirical correlation between penetration resistance and internal friction angle of sandy soils. Soils and Foundations, 36(4), 1-9, 1996

Inada M., Usage of Swedish weight sounding results. Tsuchi-to-Kiso, J. of JSSMGE 8 (1), 13-18, 1960. (in Japanese).

Iwai, S. and Ishiguro M., Applied hydro-statistics, Morikita, 1970. (in Japanese)

Japanese Society of Irrigation, Drainage and Rural Engineering, Maintenance of irrigation tanks. Guideline of land improvement designs, 2015. (in Japanese)

Katz, R.W. and Parlange, M.B., Generalization of chain-dependent processes: Application to hourly precipitation, WRR, 31(5), 1331-1341, 1995.

Kottegoda, N.T., Natale L. and Raiteri, E., Monte Carlo simulation of rainfall hyetographs for analysis and design., Journal of Hydrology, 519, 1-11, 2014.

Liu, ZJ., Xu, XF., Cheng, JQ., Wen, TF., Niu, J., Hydrological risk analysis of dam overtopping using bivariate statistical approach: a case study from Geheyan Reservoir, China, Stochastic Environmental Research and Risk Assessment, 32(9), 2515-2525, DOI: 10.1007/s00477-018-1550-0, 2018.

Minagawa, H., Masumoto, T. and Kudo, R., Development of a diurnal rainfall pattern generator incorporating characteristics of long – and short term rainfall intensity, IDRE Journal, 82(3), 15-24, 2014. (in Japanese)

Ministry of Agriculture, Forestry and Fisheries, Rural Development Bureau, Manual for evaluation of effects in land improvement projects, Taisei Publisher, 2015. (in Japanese)

National Research Institute for Earth Science and Disaster Prevention, Japan Seismic Hazard Information Station (J-SHIS), http://www.j-shis.bosai.go.jp.

Nishimura S., Shibata T., Shuku T. and Mizuma K., Risk Evaluation of earth-fills due to severe earthquakes and heavy rains, Proc. of Symposium on Reliability of Engineering Systems, 115-124, 2015.

Nishimura, S., Shuku, T. and Shibata, T., Reliability-based design of earth-fill dams to mitigate damage due to severe earthquakes, Georisk, 10(1), 83-90, DOI:10.1080/17499518.2015.1124123, 2016.

Nishimura, S., Shuku, T., Shibata, T, Evaluation of expected damage costs for earth-fill breaches due to heavy rains by response surface method, Proc. of 16ARC,TC304-014_JGS-086, CD-ROM (2019)

Nishimura, S., Takeshita, Y., Nishiyama, S., Suzuki, S., Shibata, T., Shuku, T., Komatsu, M., and Kim, B., Disaster report of 2018 July heavy rain for geo-structures and slopes in Okayama, *Soils and Foundations*, https://doi.org/10.1016/j.sandf.2020.01.009, 60(1), 300-314, 2020.

Rodriguez, C.J.T., Needham, JT. , Torres, M.A. and Bueno, E.I , A combined risk analysis approach for complex dam-levee systems, Structure and Infrastructure Engineering, 13(12), 1624-1638, DOI: 10.1080/15732479.2017.1314514, 2017.

Rubinstein, R. Y., Simulation and the Monte Carlo Method, John Wiley & Sons, 1981.

Sanmartin, F.J., Garcia, A.L, Torres, M.A. and Bueno, E.I., Empirical Tool for the Assessment of Annual Overtopping Probabilities of Dams, Journal of Water Resources Planning and Management, 145(1), DOI: 10.1061/(ASCE)WR.1943-5452.0001017**,** 2019.

Sharafati, A, and Azamathulla, H.M., Assessment of Dam Overtopping Reliability using SUFI Based Overtopping Threshold Curve, Water Resources Management, 32(7), 2369-2383, DOI: 10.1007/s11269-018-1934-4, 2018.

Shinoda M., Horii K., Yonezawa T., Tateyama M. and Koseki J., Reliability-based seismic deformation analysis of reinforced soil slopes. Soils and Foundations 46 (4): 477-490, 2006.

Toro, E.F. Riemann Solvers and Numerical Methods for Fluid Dynamics, -A Practical Introduction- 2nd Edition, Springer, 315-331, 1999.

Uzuoka, R., Sento, N., Kazama, M., Zhang, F., Yashiuma, A. and Oka, F., Three-dimensional numerical simulation of earthquake damage to group-piles in a liquefied ground, Soil dynamics and Earthquake Engineering 27, 395-413, 2007.

Wang, F. and Zhang, QL, Systemic Estimation of Dam Overtopping Probability: Bayesian Networks Approach, Journal of Infrastructures Systems, 23(2), DOI: 10.1061/(ASCE)IS.1943-555X.0000328, 2017.

Xu, Y. and Zhang, L.M., Breaching Parameters for Earth and Rockfill Dams, Journal of Geotechnical and Geoenvironmental Engineering, 135(12), 04015039, 2009.

Yoon, T. H. and Kang, S-K. Finite volume model for two-dimensional shallow water flows on unstructured grids, Journal of Hydraulic Engineering, ASCE, 78-688, 2004.

Yoshida I., Arakawa T., Kitazume T. and Otsu H., Study on seismic probabilistic safety assessment of a slope. Journal of geotechnical engineering, JSCE, No.785, 27-37, 2005. (in Japanese)

Zhang L.M., Xu, Y. and, Jia, J.S., Analysis of earth dam failures: A database approach, *Georisk*, 3(3), 184-189, 2009.

Zhong, YX., ; Guo, SL., Liu, ZJ., Wang, Y and Yin, JB., Quantifying differences between reservoir inflows and dam site floods using frequency and risk analysis methods, Stochastic Environmental Research and Risk Assessment, 32(2), 419-433, DOI: 10.1007/s00477-017-1401-4, 2018.

Table 1. Material properties of embankment materials.

| Materials | Young's modulus ($kN/m^2$) | Cohesion ($kN/m^2$) | Internal friction angle (°) | Unit weight ($kN/m^3$) | Permeability (m/s) | Poisson's ratio |
|---|---|---|---|---|---|---|
| Bs (Sat) | 12,350 | 0 | * | 20.9 | $8.55\times10^{-6}$ | 0.3 |
| Bs (Unsat) | 12,350 | 0 | * | 19.8 | $8.55\times10^{-6}$ | 0.3 |
| Ac | 1,000 | 0 | 37.4 | 15.0 | $2.71\times10^{-8}$ | 0.2 |
| Core | 16,800 | 0 | 37.4 | 20.9 | $9.95\times10^{-8}$ | 0.2 |
| Rigid soil | 16,800 | 0 | 37.4 | 20.9 | $8.55\times10^{-6}$ | 0.3 |
| Block | 16,800 | 200 | 50.0 | 23.0 | $8.55\times10^{-6}$ | 0.3 |
| Gr | 25,000,000 | 200 | 50.0 | 23.0 | $6.06\times10^{-6}$ | 0.3 |

* Predicted from SPT-*N* values

Table 2. Outline of water reservoir and probability of overflow.

| | $A$ ($km^2$) | $C\times B_s$ | $V$ (1,000$m^3$) | $A_w$($m^2$) | $h_d$(m) | $P_{fo}$ (%) |
|---|---|---|---|---|---|---|
| Original | 0.126 | 1.72 | 10.2 | 4000 | 0.66 | 0.53 |
| Restored | 0.126 | 6.70 | 8.6 | 4000 | 0.60 | 0 |

Table 3. Losses due to flood discharge.

| Items of costs for damage losses | Cost (1,000 JPY) |
|---|---|
| Farmland | 4,200 |
| Agricultural products | 9,028 |
| Houses | 105,000 |
| Private company offices | 35,961 |
| Public buildings | 4,796 |
| Agricultural storehouse | 0 |
| Business activities | 20,607 |
| Emergency repair of houses | 9,675 |
| Emergency repair of offices | 7,182 |
| Total | 196,449 |

Table 4. Risks over next 50 years.

| | Original | Restored |
|---|---|---|
| Damage probability for earthquakes | 0.6882 | 0.4294 |
| Damage probability for overflow | 0.2337 | 0.0000 |
| Total damage probability | 0.7611 | 0.4294 |
| Total risk (1,000 JPY) | 149,517 | 84,357 |

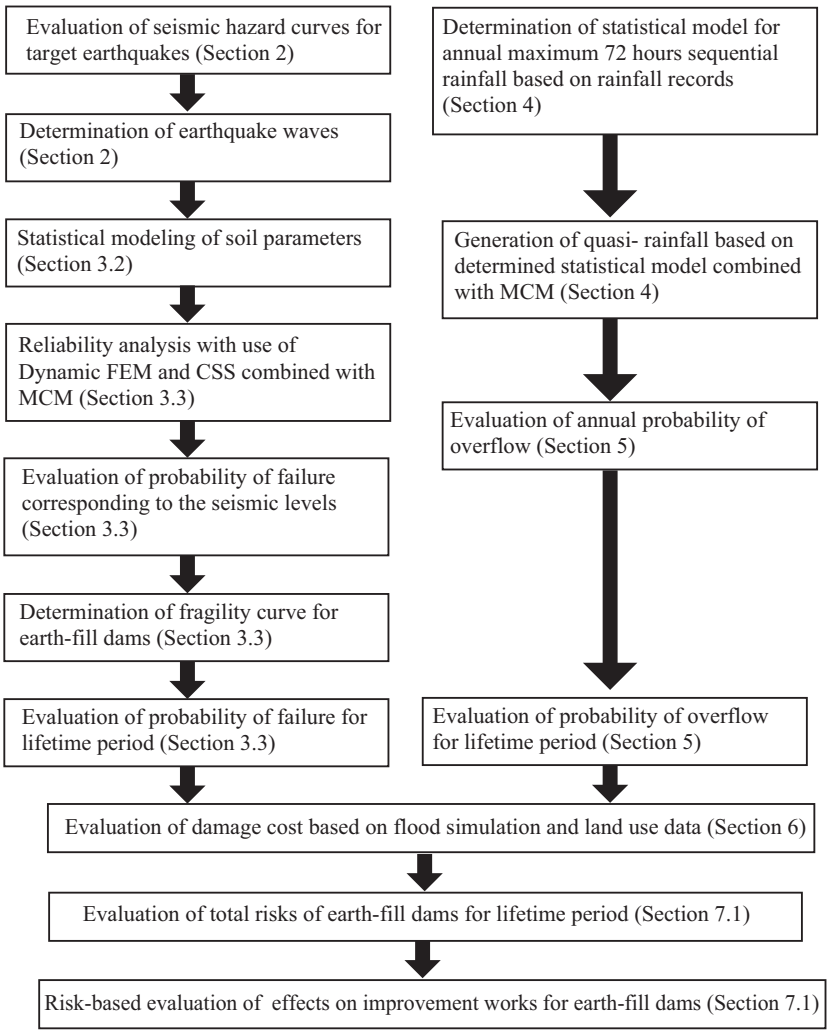


Figure 1. Flowchart of proposed approach for relaibity-based design of earth-fill dams.

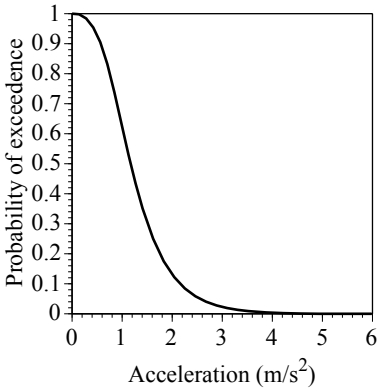


Figure 2. Earthquake hazard curve at Site H over next 50 years.

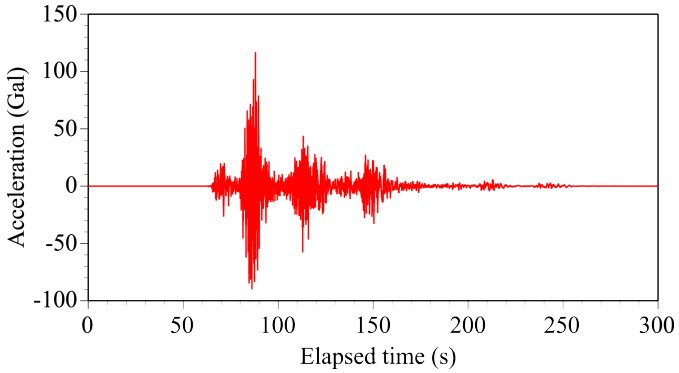


Figure 3. Sample wave due to Nankai Trough Earthquake at Site H (J-SHIS).

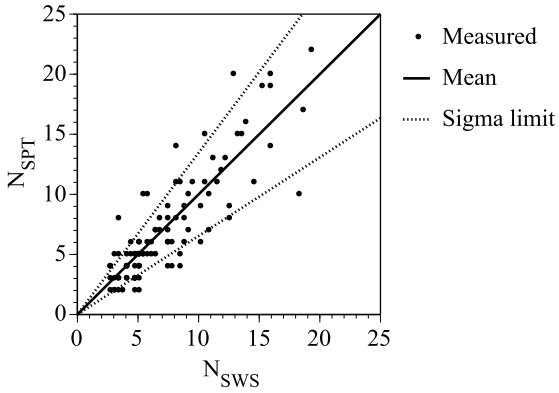


Figure 4. Relationship between SWS results and SPT *N* values.

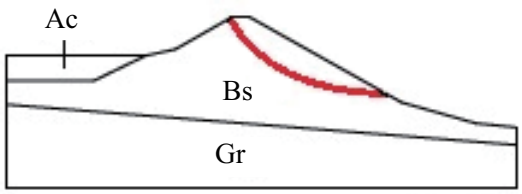


(a) Original embankment.

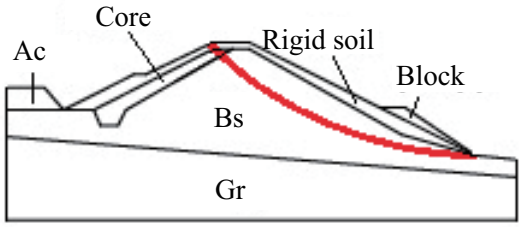


(b) Improved embankment.

Figure 5. Cross sections and critical slip surfaces of embankments.

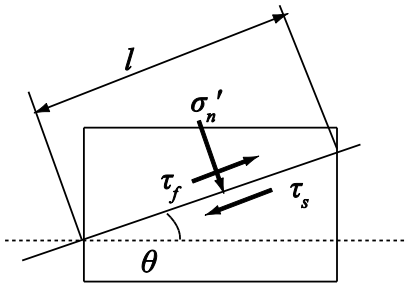


Figure 6. Slip surface across an element.

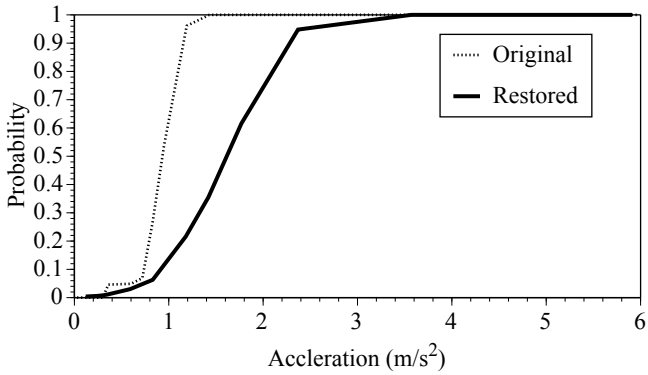


Figure 7. Fragilities of earth-fills.

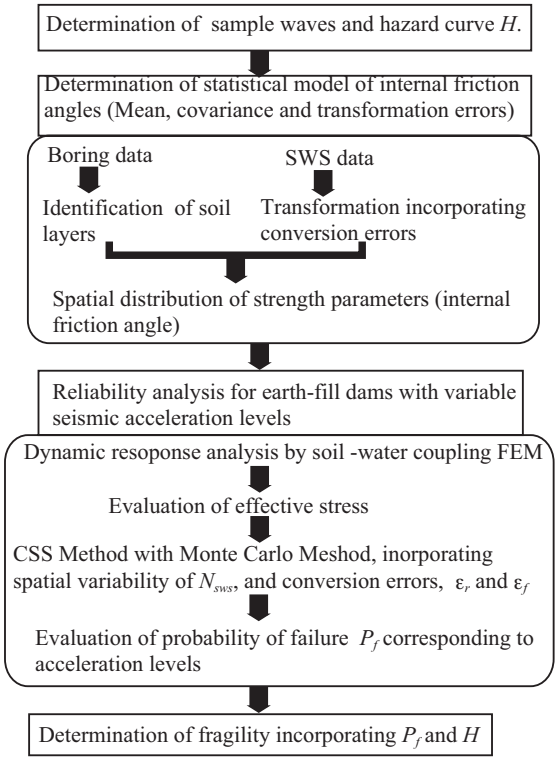


Figure 8. Flowchart of seismic reliability analysis.

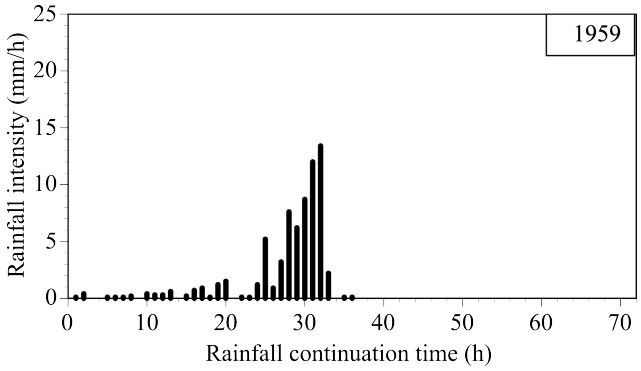


(a) Year 1959.

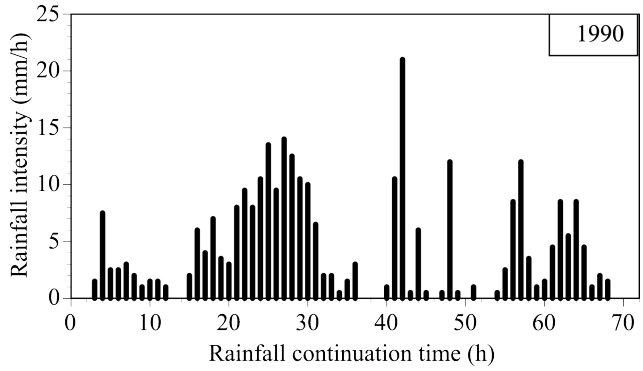


(b) Year 1990.

Figure 9. Examples of annual maximum rain of 72 hours sequence (Okayama City).

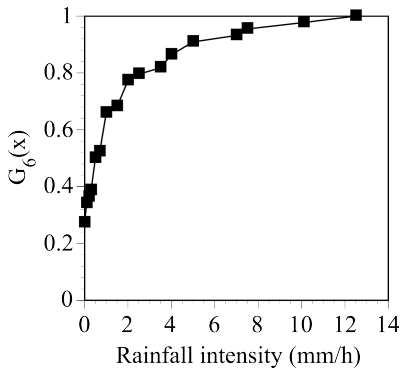


Figure 10. Cumulative probability distribution of rainfall intensity after 6 hours.

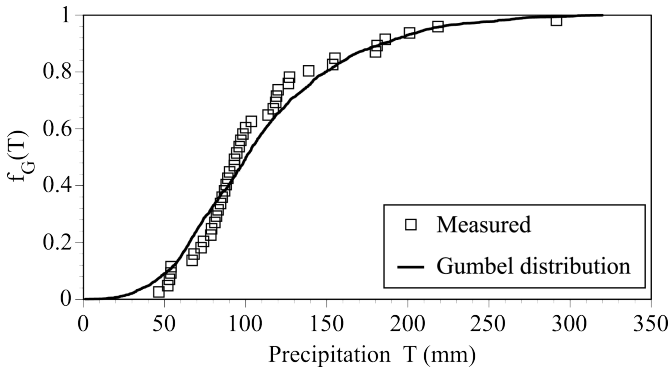


Figure 11. Cumulative distribution of maximum annual continuous precipitation of 72h.

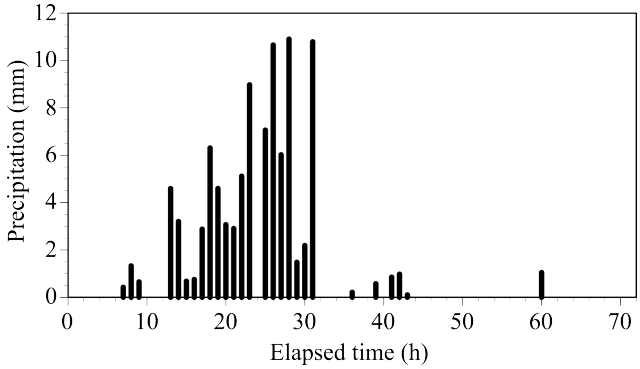


(a) Concentrating rainfall type.

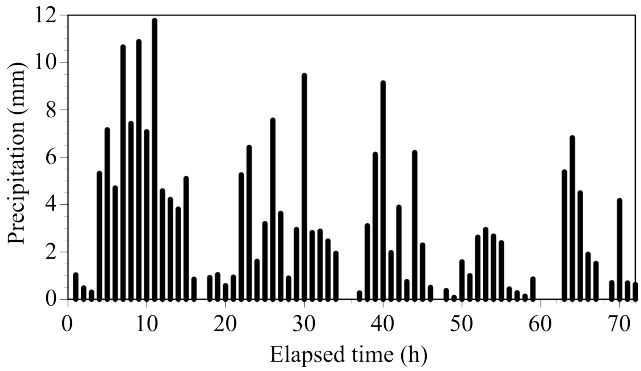


(b) Long sequential rainfall type.

Figure 12. Examples of generated quasi- precipitation.

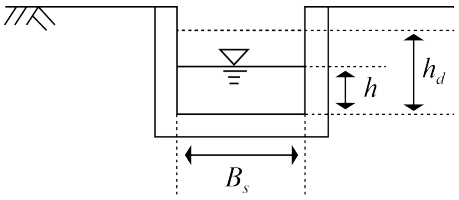


Figure 13. Definition of parameters for spillway.

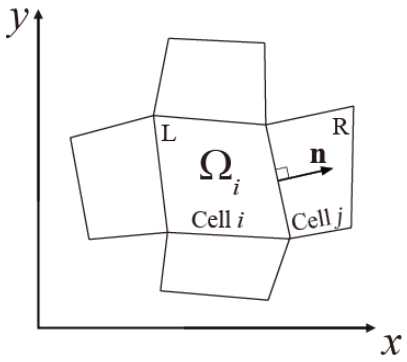


Figure 14. Typical control volume.

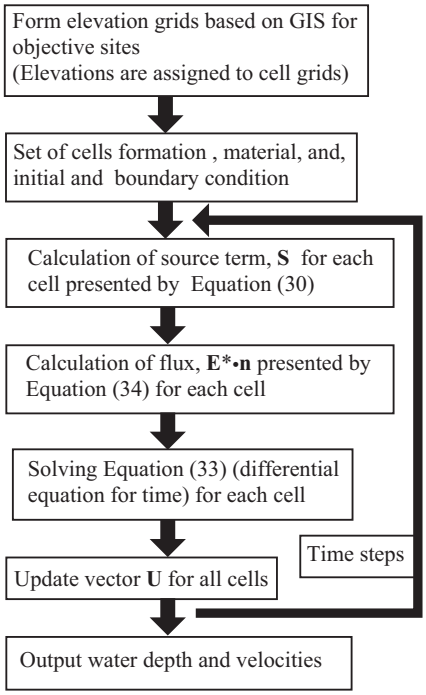


Figure 15. Flowchart of flood simulation based on FVM with HLL Rieman solver.

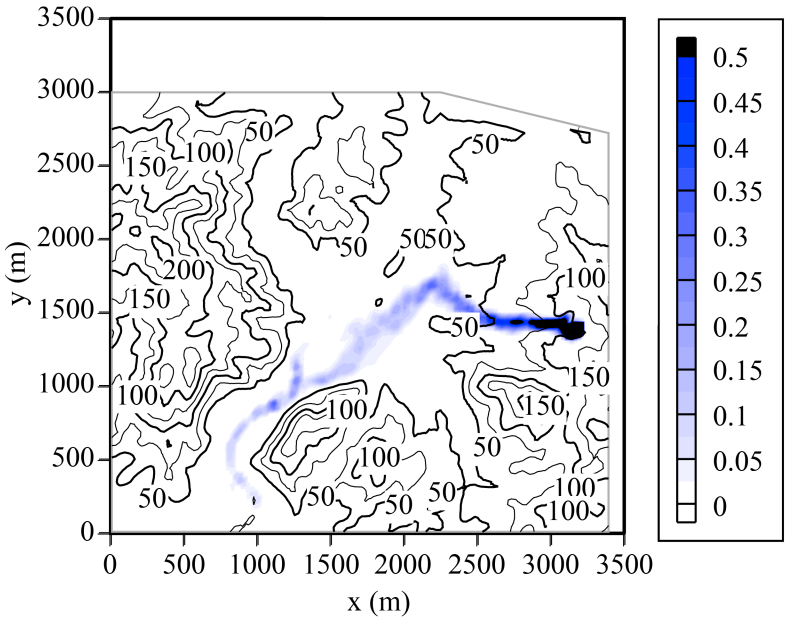


Figure 16. Submerged area and head of flood discharge (m) by dam breach.